Interactions between vortex and magnetic rings at high kinetic and magnetic Reynolds numbers

Demosthenes Kivotides

University of Strathclyde, Glasgow, Scotland, United Kingdom

(Dated: February 7, 2019)

Abstract

Interactions between magnetic and vortex rings are studied over a wide interval of interaction parameter values ranging from negligible magnetic effects on vorticity structure, to very strong effects. The employed interaction parameter measures the strength of the Lorentz force in units of the inertial force. At small interaction parameters, the vortex ring shapes part of the magnetic ring into a dissipative, curved, magnetic sheet structure. At high interaction parameters, the Lorentz force acts as an agent of proliferation of vortex rings, since it generates two vortex rings adjacent to the original magnetic structure, one of which is pulled (together with the advected magnetic field) into the wake of the original vortex ring, while the other escapes, ready to interact with another magnetic ring. Once within the initial vortex ring wake, both magnetic and vorticity structures are stretched into spirals, whilst the Lorentz force continuously generates new, intense vorticity at high magnetic field sites.

PACS numbers:

INTRODUCTION

In the magnetohydrodynamic regime, turbulence in plasmas [1, 2] involves the interaction between fluid dynamic $\mathbf{u}$, p and τ_{ij} and electromagnetic $\mathbf{A}$ fields. Here, the inertial field $\mathbf{u}$ is the flow velocity, p is the scalar pressure whose gradient acts as a *potential* (conservative) force on the flow, τ_{ij} is the viscous stress field whose divergence is a dissipative force (corresponding to entropic degrees of freedom), and $\mathbf{A}$ is the electromagnetic vector potential whose curl is the magnetic field $\mathbf{B} = \nabla \times \mathbf{A}$, whose curl is the electric current $\mathbf{J} = \nabla \times \mathbf{B}/\mu$ (where μ is the permeability of free space). The interplay between flow and electromagnetism is realized via the action of the Lorentz force $\mathbf{J} \times \mathbf{B}$ on the fluid, and via the *advection* and *stretching* of the magnetic field by the flow velocity. It is intriguing that $\mathbf{u}$ interacts with $\mathbf{A}$ only via its curl $\mathbf{B}$. This setting is reminiscent of superfluid physics [3], where the normal-fluid becomes aware of the existence of the superfluid (a scalar order parameter ψ) only via its topological defects, i.e., its vortices. In fully developed turbulence (as well as in many simpler flows) the key physical variable is the curl of $\mathbf{u}$, i.e., the vorticity $\boldsymbol{\omega} = \nabla \times \mathbf{u}$. Indeed, interactions between $\boldsymbol{\omega}$ structures [2, 4, 5] lead to interscale energy transfer and high values of small-scale strain. On the other hand, $\mathbf{B}$ coherent structures [6] are associated with key flow phenomenologies: the dynamics of linked magnetic rings illustrate the role of magnetic helicity in magnetic field decay [7] or the generation of helicity via the breakup into individual helical structures of magnetic tangles/knots of zero (initial) helicity [8]. Moreover, they play significant role in the saturation of nonlinear dynamos [9], in solar flare formation [10] (where the collision of two magnetic kinks propagating along a straight magnetic tube creates magnetic rings), stochastic particle acceleration [11], and energy dissipation [12]. Hence, $\boldsymbol{\omega}$ and $\mathbf{B}$ are "vorticities" of more primitive fields, and play a key role in the dynamics of plasma turbulence.

Indeed, from the statistical physics point of view the "problem" of turbulence can be summarized as follows: turbulence statistics are to a large extend determined by interactions between localized in space and time (coherent) $\boldsymbol{\omega}$ and $\mathbf{B}$ structures. However, localized structures leave their imprint on higher order statistics, hence, a complete statistical description of turbulence requires transport equations for higher statistical moments ("extended thermodynamics"), making such descriptions complex. On the other hand, in most cases, no such complete description is necessary but (at most) only the second

order statistics (i.e., the turbulence energy and spectra dynamics) are required. In these cases, the difficulty lies in the fact that, in order to "close" the statistical description at the second order level, an expression of third order statistics in terms of second order statistics is needed. Such a closure *cannot be simple*, since it needs to inform interscale energy transfer dynamics by encapsulating key physics encoded by higher order statistics (i.e., in essence the multiplicity of coherent structure formation, interaction and destruction events). Since the strong nonlinearity of turbulence is intractable within present mathematics, an alternative approach (employed in this Letter) is to study generic interactions between $\boldsymbol{\omega}$ and $\mathbf{B}$ ring-like structures, and, in this way, to provide physical insight for the statistical *modelling* (rather than *analysis*) of the closure problem of turbulence [13–15].

MATHEMATICAL MODEL

We analyze the standard (non-Hall [1]) incompressible MHD system, that includes the fluid momentum equation,

$$\frac{\partial \mathbf{u}}{\partial t} + \nabla\left(\frac{p}{\rho} + \frac{\mathbf{u}\cdot\mathbf{u}}{2}\right) - (\mathbf{u}\times\boldsymbol{\omega} - \widetilde{\mathbf{B}}\times\widetilde{\mathbf{J}}) - \nu\nabla^2\mathbf{u} = 0,$$

the equation for the magnetic field transport,

$$\frac{\partial \widetilde{\mathbf{B}}}{\partial t} + (\mathbf{u}\cdot\nabla)\widetilde{\mathbf{B}} - (\widetilde{\mathbf{B}}\cdot\nabla)\mathbf{u} - \lambda\nabla^2\widetilde{\mathbf{B}} = 0,$$

and the two elliptic constraints, $\nabla\cdot\mathbf{u} = 0$, and $\nabla\cdot\widetilde{\mathbf{B}} = 0$, that enforce the solenoidal character of $\mathbf{u}$ and $\widetilde{\mathbf{B}}$. Here, ρ is the fluid density, ν is the kinematic viscosity and λ is the magnetic diffusivity. The equations are written in terms of the velocity (or Alfven) units $\widetilde{\mathbf{B}} = \mathbf{B}/\sqrt{\rho\mu}$. Employing $\widetilde{\mathbf{B}}$, we can define the current $\widetilde{\mathbf{J}} = \nabla\times\widetilde{\mathbf{B}}$ and the vector potential $\widetilde{\mathbf{A}}$, so that $\widetilde{\mathbf{B}} = \nabla\times\widetilde{\mathbf{A}}$. It is also helpful to write the transport equation for $\boldsymbol{\omega}$

$$\frac{\partial \boldsymbol{\omega}}{\partial t} + (\mathbf{u}\cdot\nabla)\boldsymbol{\omega} - (\boldsymbol{\omega}\cdot\nabla)\mathbf{u} - (\widetilde{\mathbf{B}}\cdot\nabla)\widetilde{\mathbf{J}} + (\widetilde{\mathbf{J}}\cdot\nabla)\widetilde{\mathbf{B}} - \nu\nabla^2\boldsymbol{\omega} = 0,$$

where, we observe that the reaction of the magnetic field on the fluid introduces an electrodynamic term $\nabla\times(\widetilde{\mathbf{J}}\times\widetilde{\mathbf{B}})$, referred to later as the Lorentz force associated vorticity source, differentiating, in this way, the $\boldsymbol{\omega}$ and $\widetilde{\mathbf{B}}$ evolution laws. Remarkably, the magnetic effect on vorticity is the Lie derivative of $\widetilde{\mathbf{J}}$ along $\widetilde{\mathbf{B}}$, or, in tensor notation, $\mathcal{L}_B J^\mu$, $\mu = 1, 2, 3$, so

that the four inner terms in the $\boldsymbol{\omega}$ equation are $\mathcal{L}_u\omega^\mu - \mathcal{L}_B J^\mu$, whose structure corresponds to the $\mathbf{u}\times\boldsymbol{\omega} - \widetilde{\mathbf{B}}\times\widetilde{\mathbf{J}}$ term in the $\mathbf{u}$ equation. We also define the cross helicity $\mathrm{H^C} = \mathbf{u}\cdot\widetilde{\mathbf{B}}$, an inviscid flow invariant that informs about the interlinkage of vortex and magnetic tubes [1], the flux of vorticity along a vortex tube Φ, $\Phi = \int \boldsymbol{\omega}\cdot \mathrm{d}\mathbf{S} = \oint \mathbf{u}\cdot \mathrm{d}\mathbf{l}$, and the magnetic flux along a magnetic-field tube $\widetilde{\Psi}$, $\widetilde{\Psi} = \int \widetilde{\mathbf{B}}\cdot \mathrm{d}\mathbf{S} = \oint \widetilde{\mathbf{A}}\cdot \mathrm{d}\mathbf{l}$. Φ and $\widetilde{\Psi}$ are going to be referred to as "tube strengths" in the following.

METHODS AND CALCULATION SPECIFICS

The numerical methods for the solution of the model are described in great detail in reference [14], which ought to be consulted for detailed references to the literature. For completeness of exposition, we reiterate some key aspects here. The numerics employ a staggered grid, fractional step, projection, finite volume method. The spatial partial derivatives are computed with second order accurate schemes. The contribution of advective, pressure and source terms to velocity's evolution is taken into account via an explicit, third order accurate in time, low storage Runge-Kutta (RK) method. On the other hand, an implicit, second order accurate in time Crank-Nicolson (CN) scheme is applied to the viscous/diffusion terms. The CN scheme is incorporated into the RK steps and the method becomes a hybrid RK/CN scheme. In other words, the viscous stress terms are advanced via the CN scheme, but within the three Runge-Kutta time substeps rather than in one large time step. Due to the implicit nature of the CN scheme, the solution of linear algebraic systems is performed at each time step. The solenoidal conditions for velocity and magnetic fields are enforced, every time step, by projecting both fields onto the space of divergence-free vector fields (Hodge projection). The time-stepping is adaptive, satisfying the Courant-Friedrichs-Lewy (CFL) condition, and resolving viscous processes in both the Navier-Stokes and induction equations. We have written our own algorithms for this numerical analysis. A large scale description of the algorithmic aspects is available in reference [14].

All calculations have the same kinetic Reynolds number $Re_K = u\ell/\nu$, where u is a characteristic velocity, and ℓ a characteristic length scale (that is chosen to be equal to the magnetic/vortex tube diameter). We adopt a "vortex dynamical" definition of Re_K:

since Φ has $u\ell$ units, it follows that Φ/ν is an effective kinetic Reynolds number, which is set to $Re_K = 10^4$. The magnetic Prandtl number, $\mathrm{Pr}_M = \nu/\lambda$ is set equal to unity, so the magnetic Reynolds number $Re_M = u\ell/\lambda$ is equal to Re_K. Since all calculations have identical Re_K and Re_M numbers, the different physics originate in the chosen interaction parameter values $N = \nabla \times$ (Lorentz force)$/\nabla \times$ (inertial force), which scales the Lorentz force against the inertial force, hence, it indicates how important the magnetic field's action on the flow is [2]. Notably, the definition of N involves the *curl* of the inertial and Lorentz forces, rather than the forces themselves. This is because, due to the local dynamics of $\boldsymbol{\omega}$ structures, vorticity dynamics offers a more intuitive view of turbulence physics than velocity dynamics, hence, N is defined in vorticity space by taking the *curl* of the forces appearing in the momentum conservation law. In fact, employing the Lie derivatives defined above, we have $N = \| \mathcal{L}_B J^\mu \| / \| |\mathcal{L}_u \omega^\mu \|$. As shown in [14], for $Pr_M = 1$, we can write $N = \widetilde{\Psi}^2/Re_K(\lambda\ell)^2$, hence, we control N by tuning the magnetic flux $\widetilde{\Psi}$.

All computations were performed with periodic boundary conditions, which were enforced by considering the effects on $\mathbf{u}$ and $\mathbf{A}$ of vortex and magnetic tubes/rings in all adjacent boxes. In all computations the CFL number was set equal to CFL = 0.75 (for both velocity and magnetic fields). Velocity incompressibility was enforced with typical accuracy 10^{-10}, and magnetic-field incompressibility with typical accuracy 10^{-13}. The time step is chosen so that the viscous/diffusion time-scales are resolved, and was typically dictated by $\mathbf{u}$ evolution. The numerical grid for both fluid and magnetic evolutions is made of 256^3 grid points. Time is measured in units of the dissipative timescale $\tau_d = (\Delta x)^2/(6\nu)$, where Δx is the computational grid size. We present solutions of the mathematical model for three different interaction parameter values: $N = 1.5625 \times 10^{-4}$, $N = 1.5625 \times 10^2$, and $N = 6.25 \times 10^2$, which correspond to weak, significant and strong magnetic effects on the vortex structure. The radii of both rings are equal to $R = 0.2\ l_b$ (where l_b is the size of the computational domain), and the radii of their corresponding tubes are $r = 0.2\ R$. The initial configuration is shown in Fig. 1 (top, left), with the magnetic ring located at the center of the domain, and the vortex ring moving towards it.

Having written the electrodynamic variables in Alfven units, we shall drop, for simplicity, the tilde notation in the discussion of the results.

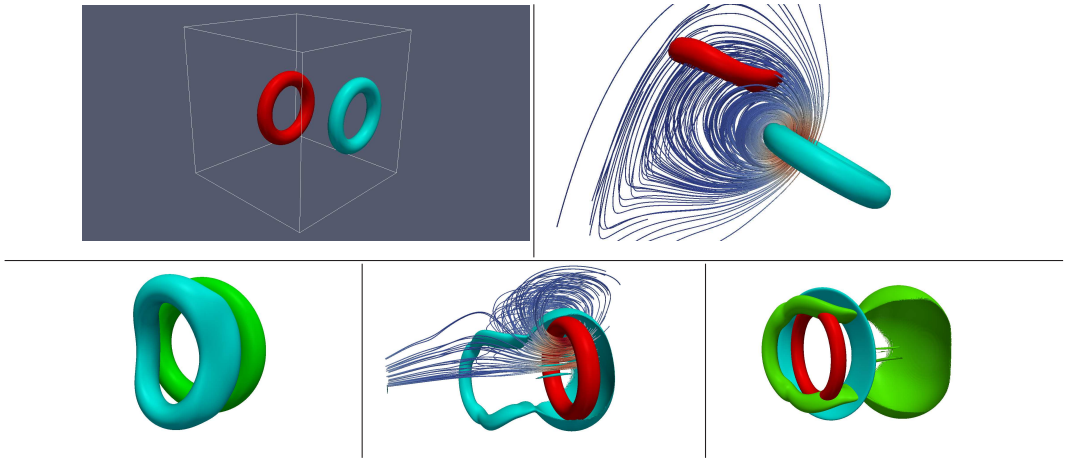

FIG. 1: $N = 1.5625 \times 10^{-4}$. **Top left**, $t = 0$: typical initial ring configuration. The magnetic flux tube (red) is located at the center of the box, and the vortex ring moves towards it. Isosurfaces drawn at half of the maximum values. **Top right**, initially tangent ring-trajectories, $t = 7.584\ \tau_d$: **B** (red) and $\boldsymbol{\omega}$ isosurfaces (drawn at half of the maximum values), as well as, velocity streamlines are shown. **Bottom left**, distant, non-colliding rings: $t = 0$ (green) and $t = 29.35\ \tau_d$ **B** isosurfaces are drawn at half of the maximum values. **Bottom middle**, colliding rings, $t = 27.85\ \tau_d$: $\boldsymbol{\omega}$ (red) and **B** isosurfaces (drawn at half of the maximum values), as well as, velocity streamlines are shown. **Bottom, right**, colliding rings: $t = 0$ (red) **B** isosurface drawn at 0.74 of maximum value, $t = 11.61\ \tau_d$ (turquoise) **B** isosurface drawn at 0.48 of maximum value, and $t = 27.85\ \tau_d$ (green) **B** isosurface drawn at 0.315 of maximum value are shown. With these three choices, all isosurfaces correspond to the same **B** field magnitude.

$N = 1.5625 \times 10^{-4}$, $Re_K = Re_M = 10^4$ SOLUTION

For completeness, three different initial configurations were studied. In all cases, since $N \ll 1$, the vortex ring remains undisturbed. In the first case, the projected ring trajectories are (initially) tangent to each other. As indicated by the velocity streamlines in Fig. 1 (top, right), the vortex flow field pushes the magnetic-ring out of the way, and contact is avoided. In the second case, the projected trajectories are distant and parallel. The vortex induces tidal effects on the flux-tube [(Fig. 1 (bottom, left)], that manifest themselves by a sideways squeezing of the flux-tube, and a displacement of the ring in the opposite to the vortex-ring motion direction. The most interesting case is when the two rings are on a collision course. Fig 2 shows the evolutions of mean magnetic energy, cross-helicity, and magnetic dissipation

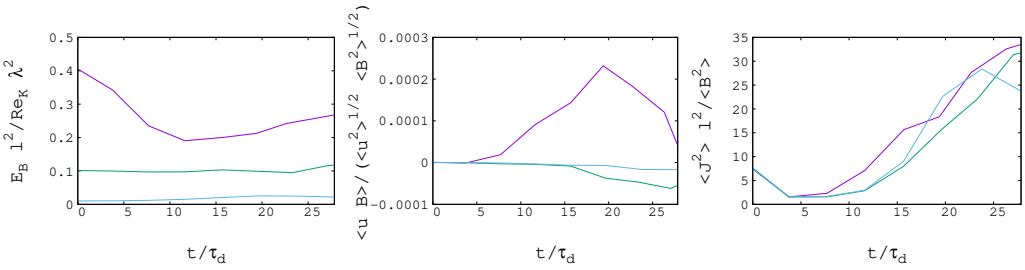

FIG. 2: Left: scaled magnetic energy $E_B = (1/\mathcal{V}) \int d\mathcal{V} \mathbf{B} \cdot \mathbf{B}$ values versus time. From bottom to top lines, the corresponding interaction parameter values are $N = 1.5625 \times 10^{-4}$ (colliding rings), $N = 1.5625 \times 10^2$, and $N = 6.25 \times 10^2$. The $N = 1.5625 \times 10^{-4}$ values have been multiplied with 10^5 in order to bring them closer to the values of the other two cases. Middle: scaled cross helicity $\mathrm{H^C} = \mathbf{u} \cdot \mathbf{B}$ values versus time. The line of smallest deviation from the zero initial value corresponds to the smallest N value, whilst the line of largest deviation to the largest N value. Right: scaled magnetic dissipation $(1/\mathcal{V}) \int d\mathcal{V} \mathbf{J} \cdot \mathbf{J}$ versus time. At time $t = 15\tau_d$, and moving upwards, we encounter the $N = 1.5625 \times 10^2$, $N = 1.5625 \times 10^{-4}$, and $N = 6.25 \times 10^2$ lines.

for this case. As indicated by the velocity streamlines in Fig. 1 (bottom, middle), the vortex flow field shapes the opposite part of the flux-tube into a curved, sheet structure with intensified magnetic energy. This corresponds to magnetic energy and dissipation increase in Fig 2, whilst the helicity shows only a very small deviation from its zero initial value.

In the magnetic energy spectra of Fig. 3 (left), sheet formation appears as an energy propagation towards high wavenumbers. This behaviour is in contrast to the kinetic energy spectra of Fig. 4 (left), where due to negligible magnetic effects, only a dissipative high wavenumber energy damping is indicated. Remarkably, the vortex flow generates new (unrelated to the original structure) magnetic fields at the centre of the vortex ring outline. Fig.1 (bottom, right), shows the gradual evolution of the flux-tube from the initial circular contour to the inflated magnetic sheet. The most distant from the vortex part of the flux-tube turns towards the vortex, whilst retaining its circular morphology. During the evolution, there was an increase of the maximum magnetic-field magnitude to a level approximately equal to 1.6 times of its initial maximum value. As shown in Table 1, in the presence of the curved magnetic sheet, there is (strain-rate stretching induced) production of magnetic energy $\langle B_i B_j S_{ij} \rangle$, and destruction of enstrophy $\langle \omega_i \omega_j S_{ij} \rangle$. The strain rate tensor eigenvalues follow the turbulence pattern, with two positive (on average) eigenvalues and

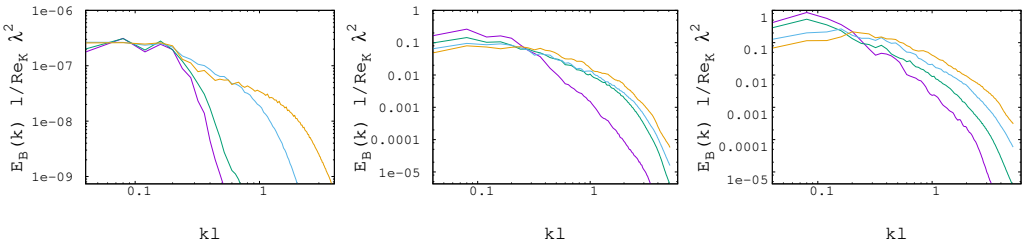

FIG. 3: Scaled magnetic energy spectra $E_B(k)$ values versus $k\ell$. Left: $N = 1.5625 \times 10^{-4}$ (colliding rings): spectra shown at $t = 3.7\ \tau_d$, $t = 7.6\ \tau_d$, $t = 15.6\ \tau_d$, and $t = 23.7\ \tau_d$. At $t = 23.7\ \tau_d$, the high k spectrum scales like $k^{-0.8}$. Middle: $N = 1.5625 \times 10^2$: spectra shown for $t = 11.5\ \tau_d$, $t = 19.6\ \tau_d$, $t = 23.3\ \tau_d$, and $t = 27\ \tau_d$. At $t = 27\ \tau_d$, the high k spectrum scales like $k^{-1.4}$. Right: $N = 6.25 \times 10^2$: spectra shown at $t = 7.7\ \tau_d$, $t = 11.6\ \tau_d$, $t = 19.6\ \tau_d$, and $t = 27\ \tau_d$. At $t = 27\ \tau_d$, the high k spectrum scales like $k^{-1.4}$ in the kl range $[0.4 - 1.2]$, whilst the low k spectrum scales like $k^{0.7}$ in the kl range $[0.04 - 0.2]$.

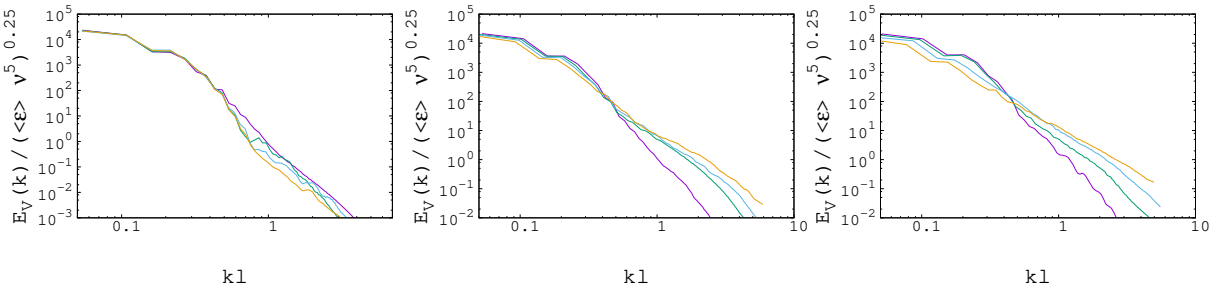

FIG. 4: Scaled kinetic energy spectra $E_V(k)$ values versus $k\ell$. The corresponding times are identical with the magnetic energy spectra times. Left: $N = 1.5625 \times 10^{-4}$ (colliding rings). Middle: $N = 1.5625 \times 10^2$: at $t = 27\ \tau_d$, there are two scaling tendencies: $k^{-3.6}$ in the wavenumber range $[0.2 - 0.8]$, and $k^{-2.4}$ in the wavenumber range $[0.9 - 2.1]$. Right: $N = 6.25 \times 10^2$: at $t = 19.6\ \tau_d$ (for which the resolution is still satisfactory), there is a $k^{-3.6}$ scaling tendency in the $k\ell$ interval $[0.2 - 0.9]$.

one negative eigenvalue, but the intermediate eigenvalue is two orders of magnitude smaller than the corresponding turbulent one.

Flow type	$\frac{\langle\lambda_1\rangle}{\langle S_{ij}S_{ij}\rangle^{1/2}}$	$\frac{\langle\lambda_2\rangle}{\langle S_{ij}S_{ij}\rangle^{1/2}}$	$\frac{\langle\lambda_3\rangle}{\langle S_{ij}S_{ij}\rangle^{1/2}}$	$\frac{\langle\omega_i\omega_j S_{ij}\rangle}{\langle\omega_i\omega_i\rangle\langle S_{ij}S_{ij}\rangle^{1/2}}$	$\frac{\langle B_iB_jS_{ij}\rangle}{\langle B_iB_i\rangle\langle S_{ij}S_{ij}\rangle^{1/2}}$
$N = 1.5625 \times 10^{-4}$	0.414637	0.000173	-0.414810	-0.4794×10^{-2}	0.06194
$N = 1.5625 \times 10^{2}$	0.4219	0.0024	-0.4243	-0.3558×10^{-2}	0.1408
$N = 6.25 \times 10^{2}$	0.4263	0.0039	-0.4302	0.1917×10^{-1}	0.1198
$N = 0$, $Re_\lambda = 10^4$	0.47	0.06	-0.53		

TABLE I: Mean values of various strain-rate tensor ($S_{ij} = \frac{1}{2}(\partial u_i/\partial x_j + \partial u_j/\partial x_i)$, $i = 1, 2, 3$) eigenvalues (λ_i) related quantities. For small to large N, the corresponding times are $t = 23.7\ \tau_d$, $t = 27\ \tau_d$, and $t = 27\ \tau_d$. The pure turbulence values shown ($N = 0$) are those of the atmospheric surface layer (at the height 10 m) [16].

$N = 6.25 \times 10^2$**,** $Re_K = Re_M = 10^4$ **SOLUTION**

As the vortex approaches the flux-tube [Fig.5 (top, left)], Lorentz force action (i.e., the Lie derivative of **J** along **B** term in $\boldsymbol{\omega}$ dynamics) induces two vortex rings at the side edges of the flux-tube, as indicated first in [14]. This appears in Fig. 2 (left) as an initial reduction of magnetic energy. Moreover, Fig.6 indicates the strongly altered (in comparison with the small N results) streamline structure, due to the Lorentz-force induced vortex rings. Subsequently [Fig.5 (top, right)], the generated vortex ring in front of the original vortex moves (with its self-induced velocity) towards the latter and reconnects with it, whilst dragging the magnetic field along its trajectory. As shown in Fig.5 (bottom, left), the generated vortex is caught by the vortical flow field of the initial ring, which cause it to rotate (anticlockwise) before getting pulled (together with the advected magnetic field) into the vortex wake where the $\boldsymbol{\omega}$ and **B** fields are stretched into a spiral-like structure [Fig.5 (bottom, right)]. In Fig. 2, these processes result in increased magnetic energy and magnetic dissipation, and (relatively strong) helicity production. On the other hand, the generated vortex ring attached to the other side of the initial flux-tube, also rotates due to the vortical flow field, but travels away from the vortex structure. Thus, we have a mechanism for the proliferation of vortex rings in plasmas, since the above process could repeat itself when the escaped ring encounters another magnetic ring. The Lorentz force generates strong vorticity (equal to five times the original vorticity values) at magnetic field locations, including new strong magnetic fields at the centre of the vortex ring, that

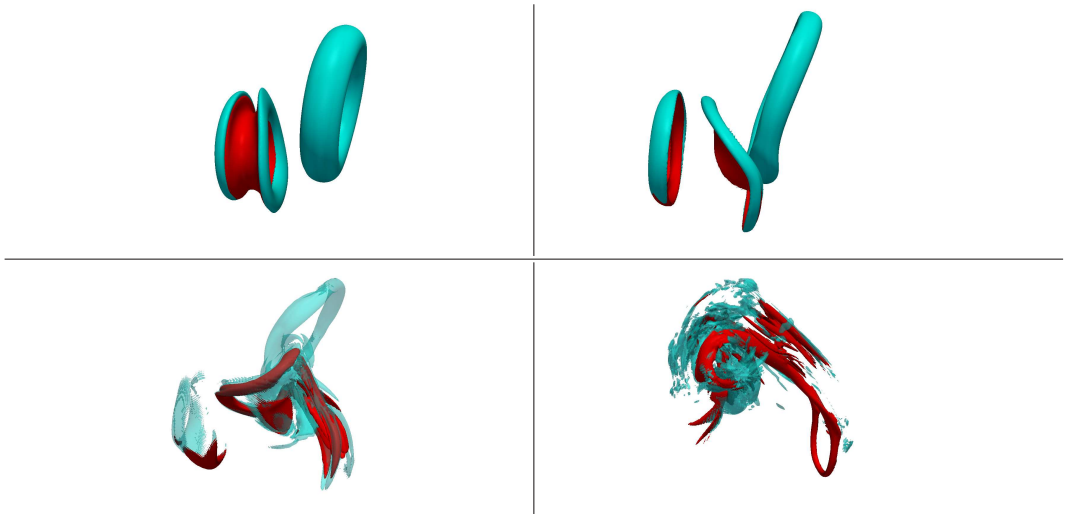

FIG. 5: $N = 6.25\times10^2$. **Top left**, $t = 7.7\ \tau_d$: $\boldsymbol{\omega}$ isosurfaces (turquoise) span levels $0.35-1$ of maximum magnitude, and $\mathbf{B}$ isosurfaces span levels $0.68-1$ of maximum magnitude. **Top right**, $t = 11.6\ \tau_d$: $\boldsymbol{\omega}$ isosurfaces (turquoise) span levels $0.405-0.5$ of maximum magnitude, and $\mathbf{B}$ isosurfaces span levels $0.55-0.88$ of maximum magnitude. **Bottom left**, $t = 19.6\ \tau_d$: an $\boldsymbol{\omega}$ isosurface (turquoise) with level equal to 0.23 of maximum magnitude, and $\mathbf{B}$ isosurfaces spanning the interval $0.33-0.5$ of maximum magnitude are shown. **Bottom, right**, $t = 27\ \tau_d$: $\boldsymbol{\omega}$ isosurfaces (turquoise) span levels $0.24-0.63$ of maximum magnitude, and $\mathbf{B}$ isosurfaces span the interval $0.36-0.65$ of maximum magnitude.

are unrelated with the original magnetic structure. The maximum magnetic field value also increases during spiral structure formation, so that, at time $t = 27\ \tau_d$, is equal to 2.3 times the initial maximum value.

In this context, it is useful to observe the evolution of scaled mean enstrophy $\Omega = (1/2\mathcal{V})\int d\mathcal{V}\ \boldsymbol{\omega}\cdot\boldsymbol{\omega}$, and scaled mean magnetic energy $E_B = (1/\mathcal{V})\int d\mathcal{V}\mathbf{B}\cdot\mathbf{B}$. The scaling factors are the corresponding values at $t = 0$. Notably, since all calculations involve the same flow field, all enstrophy values are scaled with same $\Omega(0)$. On the other hand, $E_B(0)$ is very different from case to case, with higher values corresponding to higher interaction parameters. The results (Fig. 7, left) indicate the strong enstrophy generation processes corresponding initially to vortex ring creation at the magnetic tube locations, and subsequently to enstrophy creation within the wake of the initial vortex ring. The E_B results (Fig. 7, right) show a dominant magnetic energy increase only in low N case, due

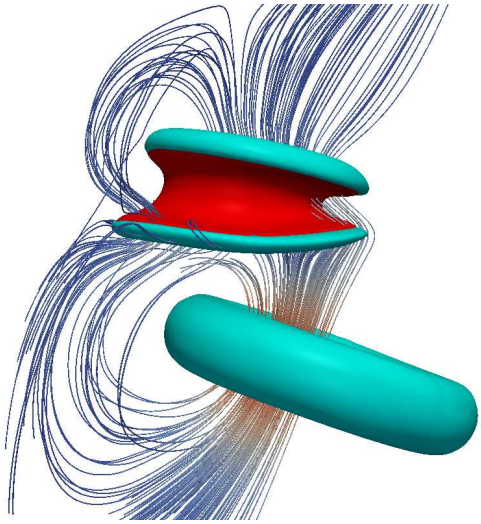

FIG. 6: $N = 6.25 \times 10^2$. Vorticity (turquoise) and magnetic field (red) isosurfaces at $t = 7.7\ \tau_d$. Isosurface levels are same as in Fig.5 (top, left), but the setting is similar to that of Fig.1 (top, right), to enable, by showing the velocity streamlines, to indicate the effect on the flow of the Lorentz-force created vortex rings during strong interactions.

to magnetic sheet formation there. In the other N cases, there is E_B production within the wake of the vortex ring, but, especially in the high N case, the initial production of vortical excitations in the flow by the Lorentz force corresponds to a significant decrease in magnetic energy levels. As shown in Fig. 3 and Fig. 4, both magnetic and kinetic energy spectra propagate towards high wavenumbers, and, in the magnetic case, there is an interesting upward slope formation at low k. Table 1 indicates production of both magnetic energy and enstrophy via strain rate induced stretching, a fact consistent with the spiral-forming process depicted in Fig.5 (bottom, right). Interestingly, and in comparison to the small N case, the intermediate eigenvalue has moved up towards its corresponding turbulence value by an order of magnitude.

$N = 1.5625 \times 10^2$, $Re_K = Re_M = 10^4$ SOLUTION

The results are indicative of the transition from the small N to the large N dynamics. Indeed, as shown in Fig.8, the phenomenology is a mixture of the small and large N

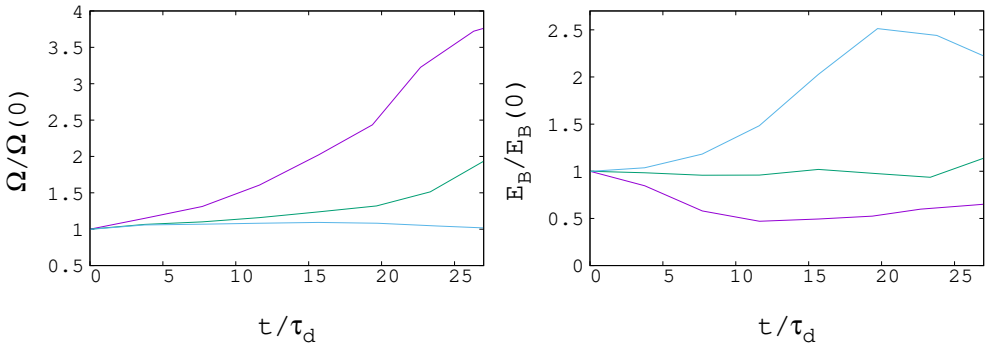

FIG. 7: Left: Scaled mean enstrophy $\Omega = (1/2\mathcal{V}) \int d\mathcal{V}\ \boldsymbol{\omega} \cdot \boldsymbol{\omega}$ versus time. The initial Ω value serves as a scaling factor. From bottom to top lines, the corresponding interaction parameter values are $N = 1.5625 \times 10^{-4}$ (colliding rings), $N = 1.5625 \times 10^{2}$, and $N = 6.25 \times 10^{2}$. Right: Scaled mean magnetic energy $E_B = (1/\mathcal{V}) \int d\mathcal{V} \mathbf{B} \cdot \mathbf{B}$ versus time. The initial E_B values serve as scaling factors. From top to bottom lines, the corresponding interaction parameter values are $N = 1.5625 \times 10^{-4}$ (colliding rings), $N = 1.5625 \times 10^{2}$, and $N = 6.25 \times 10^{2}$.

cases. In particular, the Lorentz force is strong enough to alter the vorticity field, but not to a similar extend with the larger N case. Here, the vortical structures generated at the flux-tube edges are more like sheets [Fig.8 (top, left)] than rings, hence there is no discernible independent motion towards the incoming vortex. Hence, as in the *small* N case, the vortex shapes the opposing magnetic ring into a curved sheet [Fig.8 (top, right)]. However, as in the *largest* N case, the part of the flux-tube not participating in magnetic sheet formation, is eventually pulled into the wake of the vortex ring [Fig.8 (bottom, left)], forming spiral structures [Fig.8 (top, right)] which generate (via Lorentz force action) collocated vorticity, that, in turn, interacts and changes the morphology of the vortex ring [Fig.8 (top, right)]. In Fig. 2, these processes result in a mild magnetic energy increase, strong magnetic dissipation growth, and discernible helicity production.

The magnetic spectra of Fig.3 (middle) explain why the magnetic energy increase is mild: it is the sum of a small scale production process (via strain induced stretching, as indicated in Table 1), and a large scale energy sink process which corresponds to the generation of new vorticity structures. Moreover, new magnetic field generation (unrelated to the initial magnetic flux-tube), takes place in the centre of the vortex wake. The maximum $\boldsymbol{\omega}$ magnitude increases to approximately four times its value at $t = 0$, whilst the maximum $\mathbf{B}$ magnitude increases to approximately 1.74 times its value at $t = 0$. The

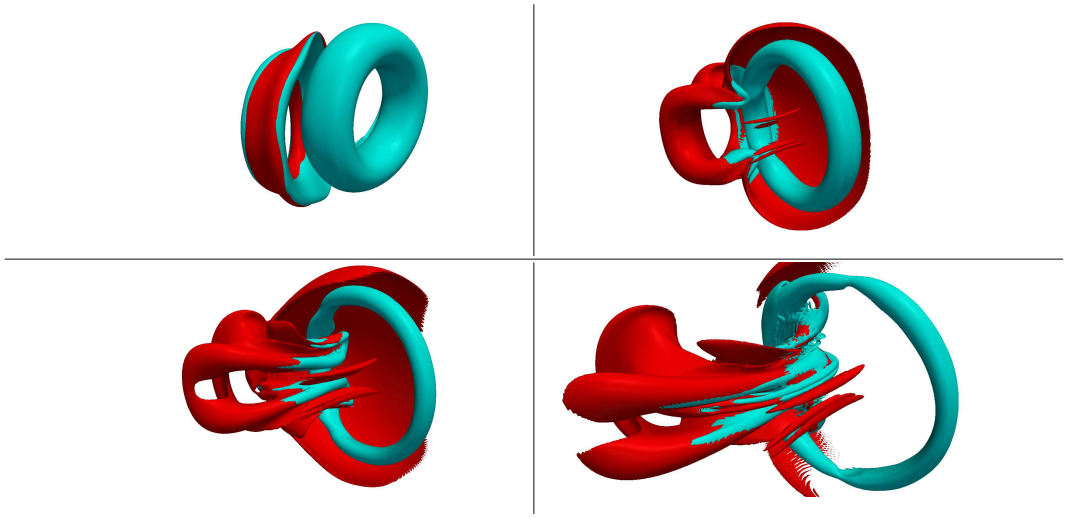

FIG. 8: $N = 1.5625 \times 10^2$. **Top left**, $t = 11.5\ \tau_d$: $\boldsymbol{\omega}$ isosurfaces (turquoise) span levels $0.13 - 0.47$ of maximum magnitude, and a single $\mathbf{B}$ isosurface is drawn at level 0.5 of maximum magnitude. **Top right**, $t = 19.6\ \tau_d$: $\boldsymbol{\omega}$ isosurfaces (turquoise) span levels $0.33 - 1$ of maximum magnitude, whilst $\mathbf{B}$ isosurfaces span levels $0.33 - 0.52$ of maximum magnitude. **Bottom left**, $t = 23.3\ \tau_d$: a single $\boldsymbol{\omega}$ isosurface (turquoise) is drawn at level equal to 0.4 of maximum magnitude, whilst $\mathbf{B}$ isosurfaces span the interval $0.17 - 0.6$ of maximum magnitude. **Bottom right**, $t = 27\ \tau_d$: $\boldsymbol{\omega}$ isosurfaces (turquoise) span levels $0.22 - 0.1$ of maximum magnitude, whilst $\mathbf{B}$ isosurfaces span levels $0.2 - 0.68$ of maximum magnitude.

enstrophy generation appears in the spectra of Fig.4 (middle) as a propagation of energy towards high wavenumbers. The results of Table 1 share with the small N case the negative (strain-rate induced) production of enstrophy, whilst, at the same, share with the largest N case (relatively) high intermediate eigenvalues. Notably, strain-rate stretching induced magnetic energy production is even stronger here than in the higher N case.

CONCLUSIONS

Due to the key role of ringlike structures in magnetic and vorticity dynamics of magnetohydrodynamic plasmas, we have analysed magnetic and vortex ring interactions over a wide range of interaction parameter N values, when the magnetic and kinetic Reynolds numbers are high.

For small N values, we are in the kinematic regime and the vortex ring propagates freely. On the other hand, the magnetic ring presents the phenomenology of a passive vector field that is shaped by tidal vortex velocity field effects. When the magnetic ring is far away from the vortex, it presents a sideways squeezing and shape deformation, whilst when the two structures collide, highly dissipative, curved magnetic sheets are formed. These sheets correspond to a cascade of magnetic-field energy to small scales and associated wavenumber space scalings.

For large N values the situation is very different: the Lorentz force induces two new vortex rings on the front and back sides of the magnetic ring plane, which move because of two factors: (a) their self induced velocities (which point towards opposing directions), and (b) the trasport action of the initial vortex ring velocity field. As a result, the generated vortex ring in front of the initial vortex moves towards the latter, and is swallowed (together with the magnetic field that it carries) by its wake, a process that creates Lorentz force induced small scale flow modes. The wake is also characterized by stretched magnetic field structures that correspond to an increase of the magnetic energy in the high wavenumber regime. The second induced vortex ring is also rotated around the initial vortex, but due to its self-induced velocity and its initial distance from the latter it escapes its pull. So in a sense, high N interaction generates new vortical modes that originate in the existing magnetic structure and breakway from the initial setting.

A future task would be to identify the above processes and spectral scaling tendencies in turbulent magnetohydrodynamic flow fields, and, in this way, explain some of the high N plasma phenomenology.

ACKNOWLEDGEMENTS

I am grateful to Tony Leonard for useful discussions during the course of this research.

[1] D. Biskamp, *Magnetohydrodynamic turbulence* (Cambridge University Press, Cambridge, 2003).

[2] P.A. Davidson, *Turbulence* (Oxford University Press, Oxford, 2004).

[3] D. Kivotides, Phys. Fluids **26**, 105105 (2014).

[4] D. Kivotides, Phys. Rev. Lett. **96**, 175301 (2006).

[5] D. Kivotides, A. Leonard, Phys. Rev. Lett. 90, 234503 (2003).

[6] V. Carbone, P. Veltri, A. Mangeney, Phys. Fluids A **2**, 1487 (1990).

[7] F. Del Sordo, S. Candelaresi, A. Brandenburg, Phys. Rev. E **81**, 036401 (2010).

[8] S. Candelaresi, A. Brandenburg, Phys. Rev. E **84**, 016406 (2011).

[9] E. L. Rempel, A. C.-L. Chian, A. Brandenburg, P. R. Munoz, S. C. Shadden, J. Fluid Mech. **729**, 309 (2013).

[10] J. I. Sakai, K. Nishi, I. V. Sokolov, Astrophys. J. **576**, 519 (2002).

[11] K. Arzner, B. Knaepen, D. Carati, N. Denewet, L. Vlahos, Astrophys. J. **637**, 322 (2006).

[12] V. Zhdankin, S. Boldyrev, J. C. Perez, S. M. Tobias, Astrophys. J. **795**, 127 (2014).

[13] D. Kivotides, A. J. Mee, C. F. Barenghi, New J. Phys. **9**, 291 (2007).

[14] D. Kivotides, Phys. Rev. Fluids **3**, 033701 (2018).

[15] D. I. Pulin, P. G. Saffman, Annu. Rev. Fluid Mech. **30**, 31 (1998).

[16] A. Tsinober A., *An informal introduction to turbulence* (Kluwer Academic Publishers, Amsterdam, 2001).